

ELECTRONIC SUPPLEMENTARY INFORMATION

Materials. 1,2-Dioleoyl-*sn*-Glycero-3-phosphoethanolamine (molecular mass 744.03 amu, purity > 99%) and 1,2-Dioleoyl-*sn*-Glycero-3-Phosphocholine (molecular mass 786.11 amu, purity > 99%) were obtained from Avanti Polar Lipids (Birmingham, AL, USA). Chloroform, HPLC-grade solvent (molecular mass 119.38 amu, purity > 99.9%), used to prepare the lipid films was purchased from Merck (Darmstadt, Germany). Heavy water, (D₂O, isotopic enrichment >99.8%, molecular mass 20.03 amu) used to prepare solutions for SANS measurements was purchased from Aldrich and used under a protective N₂ atmosphere. Double distilled and degassed water, H₂O, obtained starting from partially demineralized water was used for preparing all solutions for the other investigations. All these stuffs were used as received, without any further purification.

Preparation of the supramolecular aggregates. Dispersions of (DOPC/DOPE)/DOPURu at equimolecular concentration of both the phospholipids and at several different ratios between the phospholipid mixture and the metal-based unimer were prepared. For all the systems investigated the total concentration of DOPC/DOPE was kept at the constant value of 0.2 mmol kg⁻¹, whereas the DOPURu concentration was set consistently to the prefixed ratio. All the dispersions were prepared by direct weight of all the components.

In particular, each dispersion was prepared by dissolving suitable amounts of DOPC, DOPE and DOPURu in chloroform. The process was favored by a slight warming (~40°C) and a very short sonication treatment (~5 min). Samples to be analyzed by EPR also included 1% (wt/wt) of spin-labeled phosphatidylcholine (1-palmitoyl-2-[5-(4,4-

dimethyloxazolidine-N-oxyl)]stearoyl-*sn*-glycero-3-phosphocholine, 5-PCSL), purchased from Avanti Polar Lipids and stored at $-20\text{ }^{\circ}\text{C}$ in ethanol. Subsequently, the solution was transferred in round-bottom glass tubes and a thin film of the solutes was obtained through evaporation of the solvent with dry nitrogen gas and vacuum desiccation. The film was then hydrated with H_2O (or D_2O for SANS measurements) and the obtained suspensions were sonicated and repeatedly extruded through polycarbonate membranes of 100 nm pore sized, for at least 11 times.

SANS Measurements. Small Angle Neutron Scattering measurements were performed at $25\text{ }^{\circ}\text{C}$ with the KWS2 instrument located at the Heinz Maier-Leibnitz neutron source of the Jülich Centre for Neutron Science (Garching, Germany). Neutrons with an average wavelength of 7 \AA and 19 \AA and a wavelength spread $\Delta\lambda/\lambda \leq 0.2$ were used. A two-dimensional 128×128 array scintillation detector at two different collimation (C)/sample-to-detector(D) distances (C_8D_8 and C_8D_2 , with all the lengths express in m) measured neutrons scattered from the samples. These configurations allowed collecting data in a range of the scattering vector modulus $q = 4\pi/\lambda \sin(\theta/2)$ located between 0.0025 and 0.163 \AA^{-1} , with θ scattering angle. The obtained raw data were then corrected for background and empty cell scattering. Detector efficiency corrections, radial average and transformation to absolute scattering cross sections $d\Sigma/d\Omega$ were made with a secondary plexiglass standard.^{1,2}

DLS Measurements. Dynamic light scattering investigations were performed with a setup composed by a Photocor compact goniometer, a SMD 6000 Laser Quantum 50 mW light source operating at 5325 \AA and a PMT and correlator obtained from *Correla-*

tor.com. All the measurements were performed at $(25.00 \pm 0.05)^\circ\text{C}$ by using a thermostat bath.

In DLS, the intensity autocorrelation function $g^{(2)}(t)$ is measured and related to the electric field autocorrelation $g^{(1)}(t)$ by the Siegert relation³

$$g^{(2)}(t) = 1 + \beta |g^{(1)}(t)|^2 \quad (\text{S11})$$

where $\beta \leq 1$ is the coherence factor, which accounts for deviation from ideal correlation and depends on the experimental geometry. The parameter $g^{(1)}(t)$ can be written as the Laplace transform of the distribution of the relaxation rate Γ used to calculate the translational diffusion coefficient D

$$g^{(1)}(t) = \int_{-\infty}^{+\infty} \tau A(\tau) \exp\left(-\frac{t}{\tau}\right) d\ln \tau \quad (\text{S12})$$

Where $\tau = 1/\Gamma$. Laplace transforms were performed using a variation of CONTIN algorithm incorporated in Precision Deconvolve software. From the relaxation rates, the z -average of the diffusion coefficient D may be obtained as⁴

$$D = \lim_{q \rightarrow 0} \frac{\Gamma}{q^2} \quad (\text{S13})$$

where $q = 4\pi n_0 / \lambda \sin(\theta/2)$ is the modulus of the scattering vector, n_0 is the refractive index of the solution, λ is the incident wavelength and θ represents the scattering angle. Thus D is obtained from the limit slope of Γ as a function of q^2 , where Γ is measured at different scattering angles.

EPR Measurements. EPR spectra of 5-PCSL in (DOPC/DOPE)/DOPURu dispersions were recorded on a Elexys E-500 EPR spectrometer from Bruker (Rheinstetten, Germany) operating in the X band. Sealed capillaries containing the samples were placed in a standard 4 mm quartz sample tube. The temperature of the sample was regulated at 25 °C and maintained constant during the measurement by blowing thermostated nitrogen gas through a quartz Dewar. The instrumental settings were as follows: sweep width, 120 G; resolution, 1024 points; modulation frequency, 100 kHz; modulation amplitude, 1.0 G; time constant, 20.5 ms; sweep time, 42 s; incident power, 5.0 mW. Several scans, typically 16, were accumulated to improve the signal-to-noise ratio.

Analysis of the spectra was done according to well established methods reported in the literature.⁵ Particularly, the order parameter, S , and the Nitrogen hyperfine coupling constant, a'_N , were determined. S is related to the angular amplitudes of motion of the label, which in turn reflect the motion of the acyl chain segment to which the label is bound. In particular, S was calculated according to the relation⁶

$$S = \frac{(T_{\parallel} - T_{\perp}) a_N}{(T_{zz} - T_{xx}) a'_N} \quad (\text{SI4})$$

where T_{\parallel} and T_{\perp} are two phenomenological hyperfine splitting parameters which can be determined experimentally from the spectra. T_{xx} and T_{zz} are the principal elements of the real hyperfine splitting tensor in the spin Hamiltonian of the spin-label, which can be measured from the corresponding single-crystal EPR spectrum and are reported in the literature (T_{xx} =6.1 G and T_{zz} =32.4 G, ref. 36). a_N and a'_N are the isotropic hyperfine

coupling constants for the spin-label in crystal state and in the membrane, respectively, given by:

$$a_N = \frac{1}{3}(T_{zz} + 2T_{xx}) \quad (\text{SI5})$$

$$a'_N = \frac{1}{3}(T_{\parallel} + 2T_{\perp}) \quad (\text{SI6})$$

The isotropic hyperfine coupling constant is an index of the micropolarity experienced by the nitroxide, and the a_N/a'_N ratio in equation (SI4) corrects the order parameter for polarity differences between the crystal state and the membrane.

Cryo-TEM Measurements. Cryogenic-transmission electron microscopy (cryo-TEM) images were carried out at the Center for Chemistry and Chemical Engineering in Lund, Sweden, on a Philips CM120 BioTWIN Cryio electron microscope operating at 120 kV. A small drop of the sample solution was applied on a copper EM grid with a holey carbon film, and excess solution was blotted with a filter paper, leaving thus a thin sample film spanning the holes in the carbon film. Sample preparation was carried out in a controlled environment vetrification (CEVS) system to avoid water evaporation and to ensure cryo-fixation of the specimen at a controlled temperature (25 °C).^{7, 8}

Scattering models used for data analysis. Structural parameters of the aggregates have been obtained by applying the appropriate model to the experimental SANS data. Generally speaking, scattering cross sections $d\Sigma/d\Omega$ containing information on interactions, size and shapes of aggregates present in the system, can be expressed for a collection of monodisperse and dilute bodies as⁹

$$\frac{d\Sigma}{d\Omega}(q) = n_p P(q) + \left(\frac{d\Sigma}{d\Omega} \right)_{\text{incoh}} \quad (\text{SI7})$$

where n_p represents the number density of the scattering objects present in the system, and $P(q)$ is the form factor of the scattering particles, containing information on their shape, whereas $(d\Sigma/d\Omega)_{\text{incoh}}$ takes in to account for the incoherent contribution to the cross section measured, mainly due to the presence of hydrogenated molecules.

Scattering cross sections obtained for DOPC/DOPE and (DOPC/DOPE)/DOPURu 70/30 aqueous dispersions may be interpreted in terms of a collection of unilamellar liposomes, according to the power law $(d\Sigma/d\Omega) \propto q^{-2}$ found. Actually these kinds of aggregates cannot be observed in their completeness since the Guinier region of such objects falls almost completely in the USANS domain. As consequence the SANS region is characterized by this power law characteristic of the liposomal double layer. Indeed the q range spanned by the SANS measurements is such to allow regarding the liposomes as randomly oriented planar sheets, whose total cross section is ¹⁰

$$\frac{d\Sigma}{d\Omega}(q) = 2\pi(\rho_c - \rho_0)^2 S d^2 \frac{1}{q^2} \frac{\sin^2\left(\frac{qd}{2}\right)}{\left(\frac{qd}{2}\right)^2} + \left(\frac{d\Sigma}{d\Omega}\right)_{\text{incoh}} \quad (\text{SI8})$$

where d represents the plane thickness, whereas S is the plain surface per unit volume.

Scattering cross sections for mixed systems (DOPC/DOPE)/DOPURu 60/40 and 50/50 have been interpreted, according to Cryo-TEM images, as a sum of two contribution: the first arising from multilamellar vesicles, for which a theoretical expression has been developed by Kotlarchyk and Ritzau ¹¹ This model includes the evaluation of the lamellar thicknesses d_l , of the distance between the center of two subsequent lamellae l and the

number of lamellae N . The second contribution has been correlated to the presence of cubosomes belonging to the primitive $Im3m$ space group. A form factor obtained for the schematic representation of these structures reported in figure ESI3, has been developed. The SANS modeling was performed in a simplified manner by not describing the inner structure exactly as it is known. The real structure is believed to be bicontinuous, while here it has been assumed a regular lattice of bilayers housing cubic vacancies. This leads to the structure of a solid cube from which the regular lattice of cubic vacancies is subtracted. The solid cube in one dimension is described by

$$f_1(Q) = \frac{(D+d) \cdot \sin \frac{Q(D+d)}{2}}{\frac{Q(D+d)}{2}} \quad (\text{SI9})$$

The regular lattice of vacancies is described in one dimension by

$$f_2(Q) = \frac{D-Nd}{N} \cdot \frac{\sin \frac{Qd}{2}}{\sin \frac{Qd}{2N}} \cdot \frac{\sin \frac{Q(D-Nd)}{2N}}{\frac{Q(D-Nd)}{2N}} \quad (\text{SI10})$$

The meaning of the parameters is depicted in figure ESI3. The overall dimension of the cubosome is $D+d$, while the bilayer thickness is d . The number of vacancies (or repetitions) is N . When the terms are multiplied to yield a three dimensional structure, the result for the macroscopic cross section reads

$$\frac{d\Sigma}{d\Omega}(q) = \frac{\Delta^2 \rho \cdot \phi}{v} \cdot \int_{|\vec{Q}=q} d^2\vec{Q} \cdot \left(f_1(Q_x) \cdot f_1(Q_y) \cdot f_1(Q_z) - f_2(Q_x) \cdot f_2(Q_y) \cdot f_2(Q_z) \right)^2 \quad (\text{SI11})$$

This formula describes a regular lattice of vacancies inside a solid cube. Thus the bilayer walls of thickness d remain as a regular structure. For the experiment the single

colloids are not aligned and so an orientational averaging has to be performed. The additional factors $\Delta^2\rho$ and ϕ describe the contrast obtained from the scattering length density difference of the solvent and the solutes, and the volume fraction of the scattering objects, respectively. The normalization to the volume of a single cubosome $v = (D+d)^3 - (D-dN)^3$ compensates the integral being proportional to the square of this volume. So the forward scattering of the macroscopic cross section contains the contrast, the concentration and the volume of the cubosome.

A closed form of equation (SI11) can be obtained, being more convenient for computational purposes. Final expression is

$$\frac{d\Sigma}{d\Omega}(q) = \frac{\Delta^2\rho \cdot \phi}{v} \frac{\pi}{400} \cdot \sum_{j=0}^9 \sum_{k=0}^{19} \sin t \cdot [f_1(q \cdot \cos y \cdot \sin t) \cdot f_1(q \cdot \sin y \cdot \sin t) \cdot f_1(q \cdot \cos t) - f_2(q \cdot \cos y \cdot \sin t) \cdot f_2(q \cdot \sin y \cdot \sin t) \cdot f_2(q \cdot \cos t)]^2 \quad (\text{SI12})$$

where

$$t = \left(k + \frac{1}{2}\right) \frac{\pi}{40} \quad (\text{SI13})$$

$$y = \left(j + \frac{1}{2}\right) \frac{\pi}{40} \quad (\text{SI14})$$

The important property of this model is that it describes a correlation peak which is connected to the periodicity of the structure and a power law at lower scattering vectors which is connected to the compactness of the colloid.¹² The overall size is obtained at lowest scattering vectors in the Guinier regime. While the peak height, especially in relation to possibly higher order peaks, would give insight to the exact structure of the repeat unit, we simply aim at the position of first order peak which is connected to the repeat

distance. The astonishing result of the power law region at slightly lower q is that already at relatively low vacancy numbers N being $\cong 10$ a Porod like exponent of $\alpha = -4.1$ ($d\Sigma/d\Omega \propto q^{-\alpha}$) is obtained. In comparison with multilamellar vesicles the compactness came to the Porod regime for large shell numbers of $\cong 30$. Thus, the cubosome is a more compact structure compared to multilamellar vesicles.

Figure ESI3 shows a schematic plot of the cubosome form factor obtained in equation (SI12) as a function of the scattering vector modulus q . The function appears very oscillating, due to the presence of sin and cos terms. The oscillations are averaged out if D has allowed to be polydisperse, as it is. In all the fitting performed, the D parameter has been assumed to be polydisperse with a Zimm Schultz distribution function. The instrument resolution has also been taken in to account and all the fittings have been carried out with the QTIKWS software developed at the Jülich Centre for Neutron Science by one of us (V.P.).

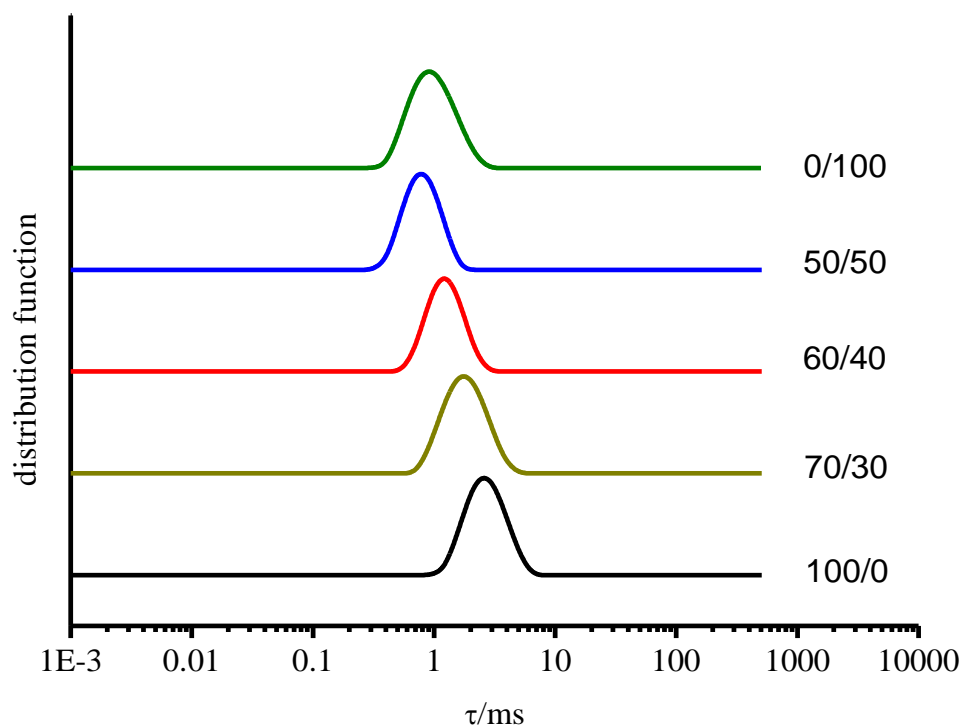


Figure ESI1 – Relaxation time distribution functions obtained at 25°C and $\theta = 90^\circ$ for the (DOPC/DOPE)/ DOPURu/ H₂O systems at different phospholipids/Ru complex molar ratios (as indicated), by means of DLS measurements.

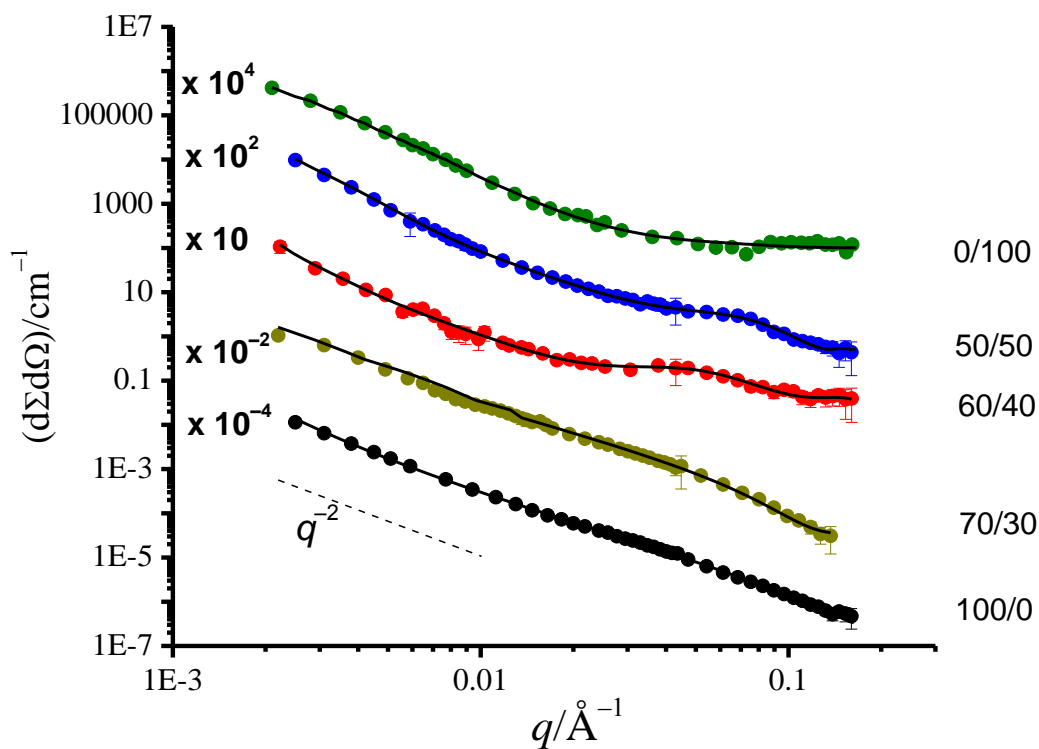


Figure ESI2 – Scattering cross sections obtained at 25°C for the aqueous dispersions (DOPC/DOPE)/DOPURu/H₂O at different ratios between the total phospholipids and the metal complex, as indicated. Fitting curves to the experimental data through the models reported in the text are reported. For a better comparison, data have been multiplied for a scale factor as displayed. A straight dashed line indicating the power law $d\Sigma/d\Omega \propto q^{-2}$ has also been drawn.

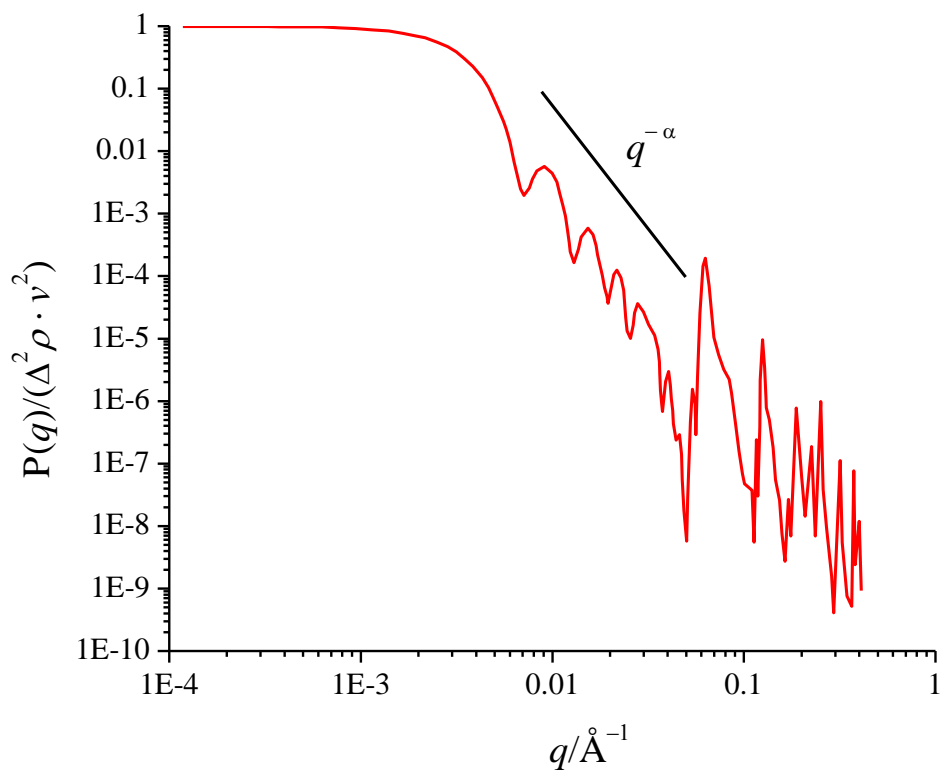


Figure ESI3 – Exemplificative plot of the form factor $P(q)$ obtained in equation (SI12), normalized for the square of the contrast $\Delta\rho = \rho_c - \rho_0$ and the volume v of a cubosome for the following set of parameters: $D = 1000 \text{\AA}$, $d = 10 \text{\AA}$, $N = 10$.

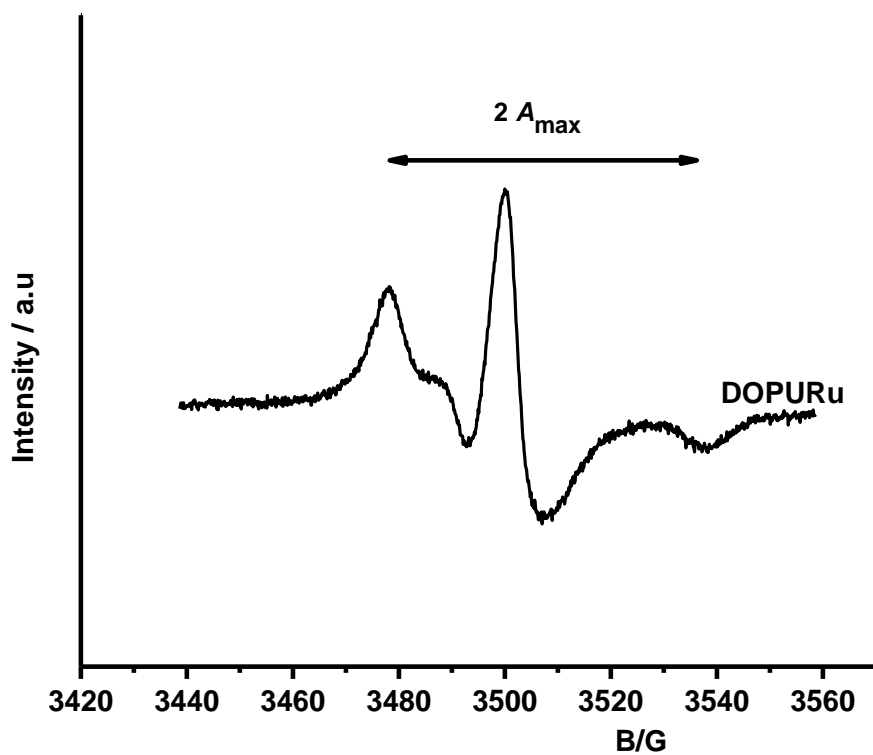


Figure ESI4. EPR spectrum obtained at 25°C for 5-PCSL inserted in DOPURu membranes, respectively.

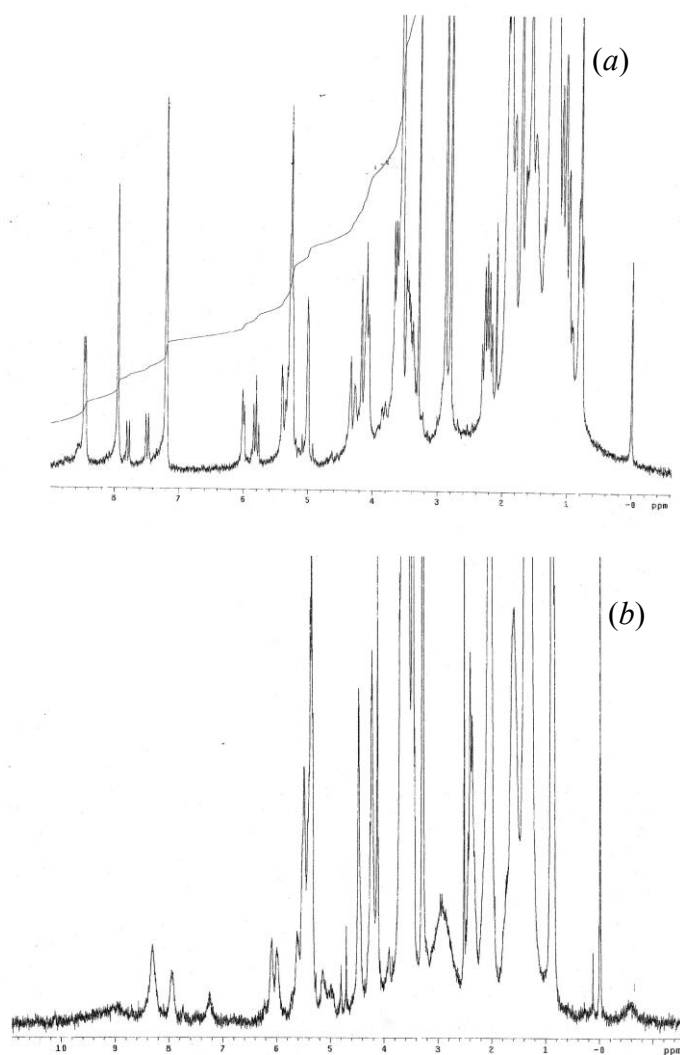


Figure ESI5. ¹H-NMR spectra obtained at 25°C for: (a) DOPU (molecule 2 reported in Scheme 1) and (b) DOPURu (molecule 3).

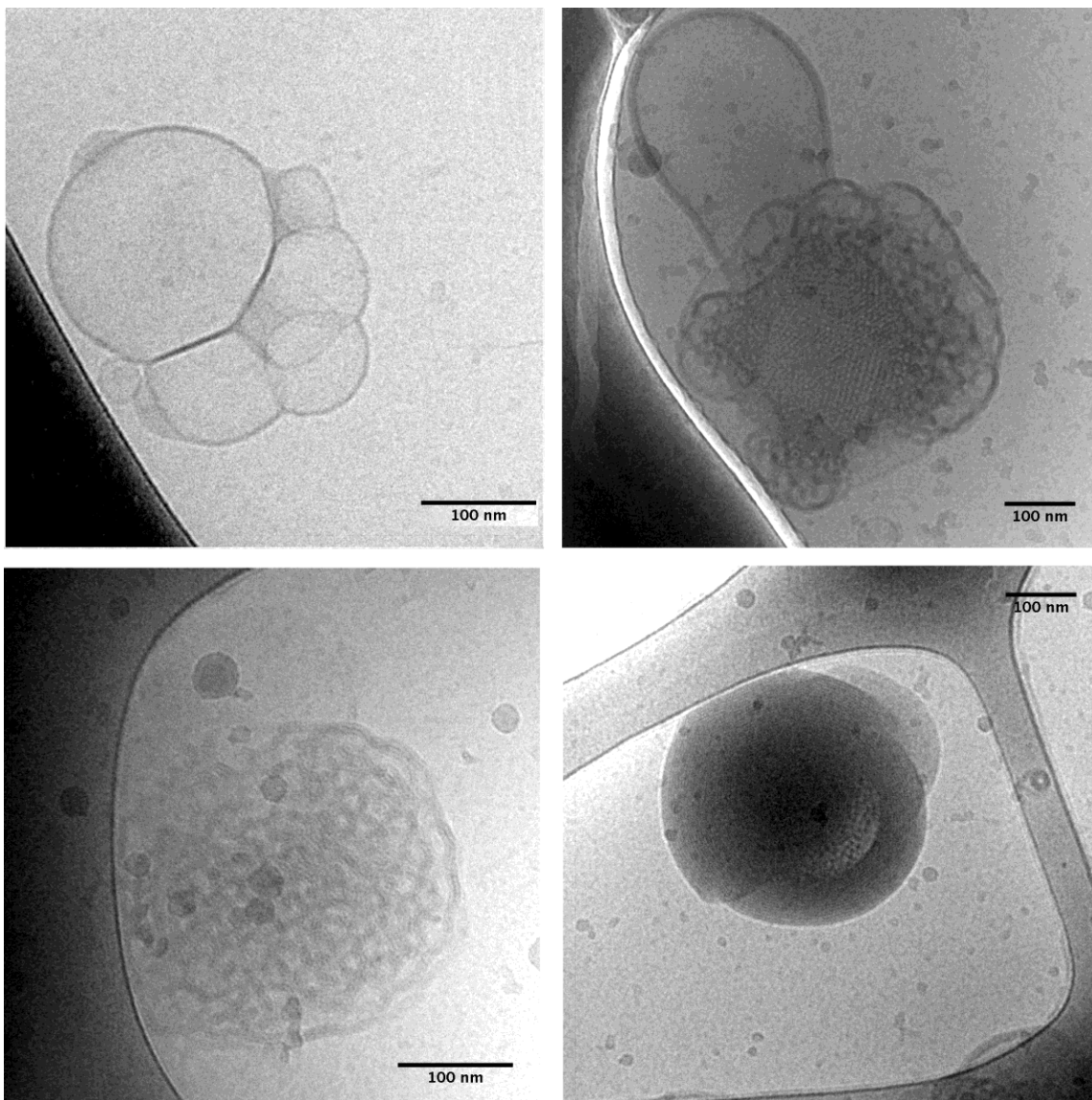


Figure ESI6. Further Cryo-TEM images obtained for (DOPC/DOPE)/ DOPURu/H₂O system at 60/40 and 50/50 phospholipids/Ru complex molar ratios. Samples show some different phases, such as multilamellar vesicles, cubosomes, as well as mixed phases. The lamellar regions of the multi-lamellar vesicles have a spacing ranged ~ 4 nm, whereas the cubic phases have a lattice parameter ranged between (9-12) nm.

TABLES.

DOPC:DOPE (1:1)/DOPURu molar ratio	$\frac{10^8 \mathcal{D}}{\text{cm}^2 \text{s}^{-1}}$	$\frac{R_h}{\text{Å}}$
0/100	3.1±0.2	700±30
50/50	2.9±0.3	750±40
60/40	2.6±0.3	850±40
70/30	2.5±0.2	880±40
100/0	1.7±0.3	1300±70

Table ESI1 – Translational diffusion coefficients \mathcal{D} and hydrodynamic radii R_h of the aggregates found in (DOPC/DOPE)/DOPURu aqueous systems. Hydrodynamic radii of the aggregates have been obtained via Stokes-Einstein equation.

(DOPC/DOPE) (1:1)/DOPURu molar ratio	$\frac{D+d}{\text{Å}}$	$\frac{d}{\text{Å}}$	N	ϕ_{cub}	N_l	$\frac{d_l}{\text{Å}}$	$\frac{l}{\text{Å}}$	ϕ_{ves}
0/100	–	–	–	–	3 ± 1	35 ± 3	50 ± 1	–
50/50	~ 1500	38 ± 4	15 ± 2	$\sim 3 \cdot 10^{-5}$	10 ± 1	30 ± 3	120 ± 12	$\sim 1 \cdot 10^{-5}$
60/40	~ 1500	40 ± 4	10 ± 1	$\sim 2 \cdot 10^{-6}$	7 ± 1	31 ± 3	120 ± 12	$\sim 1 \cdot 10^{-6}$
70/30	–	–	–	–	1	45 ± 4	–	–
100/0	–	–	–	–	1	39 ± 2	–	–

Table ESI2 – Linear dimension $D+d$, bilayer thickness d and number of water channel per side N obtained for cubosome structures in the mixed systems (DOPC:DOPE 1:1) 0.4 mmol kg⁻¹ / DOPURu by means of the scattering model developed and fitted to SANS experimental data. The dimension D is only approximately determined since the missing of the Guinier regime in the data, as well as the total volume fraction of the scattering structures. For the 100/0 and 70/30 ratios, where unilamellar vesicles are present, the bilayer thickness d_l has been reported. Further details are reported in the Supplementary Information Section.

(DOPC/DOPE 1:1)/DOPURu molar ratio	$\frac{a'_N}{\text{G}}$	S
0/100	16.2±0.6	0.69±0.04
50/50	15.5±0.4	0.64±0.03
60/40	15.3±0.3	0.61±0.02
70/30	15.2±0.3	0.60±0.02
100/0	15.2±0.3	0.60±0.02

Table ESI3 – Nitrogen isotropic hyperfine coupling constant, a'_N , and the order parameter, S , obtained from the EPR spectra of 5-PCSL dispersed in (DOPC/DOPE)/DOPURu aqueous systems.

REFERENCES

1. G. D. Wignall and F. S. Bates, *Journal of Applied Crystallography*, 1987, **20**, 28-40.
2. T. P. Russell, J. S. Lin, S. Spooner and G. D. Wignall, *Journal of Applied Crystallography*, 1988, **21**, 629-638.
3. B. J. Berne and R. Pecora, *Dynamic Light Scattering: with Applications to Chemistry, Biology, and Physics*, 1975.
4. G. A. Brehm and V. A. Bloomfield, *Macromolecules*, 1975, **8**, 663-665.
5. L. M. Gordon and C. C. Curtain, in *Advances in Membrane Fluidity I: Methods for Studying Membrane Fluidity*, eds. R. C. Aloia, C. C. Curtain and L. M. Gordon, Alan R. Liss, New York, 1988.
6. W. L. Hubbell and H. M. McConnell, *Journal of the American Chemical Society*, 1971, **93**, 314-326.
7. Y. Talmon, *Berichte der Bunsen-Gesellschaft*, 1996, **100**, 364-372.
8. M. Almgren, K. Edwards and J. Gustafsson, *Current Opinion in Colloid & Interface Science*, 1996, **1**, 270-278.
9. M. Kotlarchyk and S. H. Chen, *Journal of Chemical Physics*, 1983, **79**, 2461-2469.
10. G. Ma, D. J. Barlow, M. J. Lawrence, R. K. Heenan and P. Timmins, *Journal of Physical Chemistry B*, 2000, **104**, 9081-9085.
11. M. Kotlarchyk and S. M. Ritzau, *Journal of Applied Crystallography*, 1991, **24**, 753-758.
12. H. Frielinghaus, *Physical Review E: Statistical, Nonlinear, and Soft Matter Physics*, 2007, **76**, 051603/051601-051603/051608.